1-1-2018

Engineering Surface Amine Modifiers of Ultrasmall Gold Nanoparticles Supported on Reduced Graphene Oxide for Improved Electrochemical CO2 Reduction

Yong Zhao
University of Wollongong, yz705@uowmail.edu.au

Caiyun Wang
University of Wollongong, caiyun@uow.edu.au

Yuqing Liu
University of Wollongong, yuqing@uow.edu.au

Douglas R. MacFarlane
Monash University, douglas.macfarlane@monash.edu.au

Gordon G. Wallace
University of Wollongong, gwallace@uow.edu.au

Engineering Surface Amine Modifiers of Ultrasmall Gold Nanoparticles Supported on Reduced Graphene Oxide for Improved Electrochemical CO2 Reduction

Abstract

Ultrasmall gold (Au) nanoparticles with high mass activity have great potential for practical applications in CO2electroreduction. However, these nanoparticles often suffer from poor product selectivity since their abundant low-coordinated sites are favorable for H2evolution. In this work, a catalyst, reduced graphene oxide supported ultrasmall Au nanoparticles (≈2.4 nm) is developed which delivers high Au-specific mass activities (>100 A g-1) and good Faradaic efficiencies (32-60%) for the CO2-to-CO conversion at moderate overpotentials (450-600 mV). The efficiencies can be improved to 59-75% while retaining the ultrahigh mass activities via a simple amine-modification strategy. In addition, an amine-structure-dependent effect is revealed: linear amines promote the CO formation whereas the branched polyamine greatly depresses it; the increasing alkyl chain length boosts the promotion effect of linear amines. The strong Au-amine interaction and molecular configuration induced amine coverage on the ultrasmall Au NPs may contribute to this effect.

Keywords

graphene, oxide, improved, electrochemical, co2, reduction, amine, modifiers, ultrasmall, gold, nanoparticles, supported, engineering, reduced, surface

Disciplines

Engineering | Physical Sciences and Mathematics

Publication Details

Zhao, Y., Wang, C., Liu, Y., MacFarlane, D. R. & Wallace, G. G. (2018). Engineering Surface Amine Modifiers of Ultrasmall Gold Nanoparticles Supported on Reduced Graphene Oxide for Improved Electrochemical CO2 Reduction. Advanced Energy Materials, 8 1801400-1-1801400-9.

WILEY-VCH

DOI: 10.1002/
Article type: Full paper

Engineering Surface Amine Modifiers of Ultrasmall Gold Nanoparticles Supported on Reduced Graphene Oxide for Improved Electrochemical CO_2 Reduction

Yong Zhao, Caiyun Wang, Yuqing Liu, Douglas R. MacFarlane, Gordon G. Wallace**

Y. Zhao, Dr. C. Wang, Y. Liu, Prof. G. G. Wallace
ARC Centre of Excellence for Electromaterials Science, Intelligent Polymer Research Institute, AIIM, Innovation Campus, University of Wollongong, North Wollongong, NSW 2522, Australia
E-mail: caiyun@uow.edu.au; gwallace@uow.edu.au

Prof. D. R. MacFarlane
School of Chemistry, Monash University, Clayton, VIC 3800, Australia

Keywords: carbon dioxide reduction, molecular modification, reduced graphene oxide, gold nanoparticle, amine

Ultrasmall gold (Au) nanoparticles with high mass activity have great potential for practical applications in CO_2 electroreduction. However, these nanoparticles often suffer from poor product selectivity since their abundant low-coordinated sites are favorable for H_2 evolution. In this work, we develop a catalyst, reduced graphene oxide supported ultrasmall Au nanoparticles (~ 2.4 nm), which delivers high Au-specific mass activities (> 100 A g^{-1}) and good faradaic efficiencies (32%-60%) for the CO_2-to-CO conversion at moderate overpotentials (450-600 mV). The efficiencies can be improved to 59%-75% while retaining the ultrahigh mass activities via a simple amine-modification strategy. In addition, an amine-structure-dependent effect is revealed: linear amines promote the CO formation whereas the branched polyamine greatly depresses it; the increasing alkyl chain length boosts the promotion effect of linear amines. The strong Au-amine interaction and molecular configuration induced amine coverage on the ultrasmall Au NPs may contribute to this effect.

1. Introduction

Electrochemical reduction of CO_2 (CO_2ER) into valuable products is a promising and sustainable approach to store renewable energy and mitigate global climate change.[1] Major challenges are the poor energy efficiency and product selectivity due to the large overpotential for CO_2 activation, complicated CO_2 reduction pathway and competitive H_2 evolution reaction (HER).[2] Au is one of the best electrocatalysts that can overcome these barriers for the CO_2-to-CO conversion.[3] Nanostructured Au such as nanoparticles (NPs),[4] mesoporous inverse opals,[5] ultrathin nanowires[6] and field-enhanced needles[7] have demonstrated impressive electrocatalytic activity and selectivity. However, the majority of Au atoms are restrained in the particle core where no reaction occurs, resulting in poor utilization.

Downsizing the Au particle to sub-5 nm can significantly increase the utilization efficiency, which is highly desirable for reducing cost and promoting large-scale application.[8] Such small Au NPs are typically obtained from complicated colloidal synthesis coupled with a tedious surfactant-removal process. The residual surfactants often deteriorate the catalytic activity.[9] Moreover, the increased low-coordinated corner sites are more favorable for the competitive HER, lowering the CO selectivity.[10,4a] For example, downsizing the Au NPs to less than 4 nm on a SiO_2/Si support led to an exponential increase of current density to over 100 mA cm^{-2}, but with a limited CO faradaic efficiency (FE_{CO}) of less than 20% (at -1.2 V vs. reversible hydrogen electrode, RHE). [10]

The CO selectivity of small Au NPs may be improved by tuning their binding ability to reaction intermediates (*COOH or *CO) via tailoring the electronic structure and catalytic environment of the Au active sites.[11] Molecular modification is a simple and effective approach to achieve this goal. It has demonstrated impressive capability to tune the electrocatalytic selectivity of Au catalysts.[12] For example, a thiol-tethered pyridinium monolayer modification on Au foil improved the selectivity for formate formation via a proton-induced desorption mechanism.[12b] The phenylethanethiol-protected Au_{25} clusters

provided an anionic charge environment facilitating CO_2 adsorption and C=O bond activation, showing a promoted onset potential (< 90 mV) and a superior FE_{CO} of ~ 100% (at -1.0 V vs. RHE).[12c] The N-heterocyclic-carbene functionalized 7 nm Au NPs exhibited an improved reaction kinetics for CO formation due to the strong electronic donation from carbene to Au NP surface.[12a] Recently the adsorbed CN^- and Cl^- anions were demonstrated as promoters for CO production on Au nanostructured electrodes because of the improved stabilization of the *COOH intermediates.[12d] Amine species with the ability of promoting CO_2 adsorption and suppressing HER have great potential in this regard.[13] Their modifications have remarkably promoted the CO_2ER on Cu,[14] Ag,[15,13d] MoS_x,[13b] and N-doped carbon nanotubes.[16] However, the influence from amines with different molecular structures has not been revealed. Amine-modified Au for CO_2ER has not been reported either. Thus systematic research on amine-modified sub-5 nm Au NPs should provide not only an opportunity to remedy the selectivity problem of ultrasmall Au NPs but also a deeper insight into the effect of ligand-induced surface functionalization for CO_2ER on Au.

Herein we develop a reduced graphene oxide (rGO) sheets supported ultrasmall Au NPs catalyst for CO_2-to-CO conversion with ultrahigh mass activity and excellent selectivity. This rGO-Au composite is synthesized via a facile and surfactant-free wet chemistry method. It not only delivers a high Au utilization efficiency, but also provides a clean platform to investigate the influence of surface modification on CO_2ER. Five common primary amines with different structures are selected to modify catalysts to systematically investigate the influence of amine structures on CO_2ER. An amine-structure-dependent surface modification effect is revealed. Linear amines promote the CO formation whereas the branched polyamine greatly depresses it. Among them, the linear oleylamine exhibits the best promotion effect with more than 20% increase in CO selectivity while does not deteriorate the catalytic activity. Ultrahigh Au-specific mass activities (> 100 A g^{-1}) coupled with improved CO faradaic efficiencies (> 60%) are achieved at the moderate overpotential range of 450-600 mV.

2. Results and discussion

Partially reduced graphene oxide sheet with high surface area and abundant defective sites was used as a substrate for the growth of Au NPs. The reaction between the oxidative $AuCl_4^-$ ions and reductive O- and N-containing functional groups on rGO leads to the spontaneous formation of ultrasmall Au NPs on rGO sheets.[8a] The defective sites of rGO may act as the adsorption and nucleation sites, and their strong interactions with Au atoms lead to the stabilization of Au NPs. The formed rGO-Au composite was then modified with propylamine (PA), hexylamine (HA), oleylamine (OLA), ethylenediamine (EDA) or polyethyleneimine (PEI) to futher tune the electrocatalytic propoerties (**Figure 1**a). These amines with different molecular structures or functionality density may induce different Au-amine interactions and lead to different influence on CO_2ER.

The rGO-Au composite was investigated by X-ray diffraction (XRD), which confirmed a face-centered cubic (fcc) crystal structure of Au NPs (Figure 1b). The scanning electron microscopy (SEM) and transmission electron microscopy (TEM) studies revealed a sheet-like morphology and a uniform dispersion of Au NPs on rGO (Figure 1c-e). The size distribution of Au NPs exhibited a typical Gaussian shape with an average diameter of 2.4 nm and a narrow dispersion of 0.5 nm (inset of Figure 1e). These Au NPs were nearly spherical in shape without clearly exposed facets (high-resolution TEM image, HRTEM, Figure 1f). The discerned lattice spacing of 0.23 nm can be ascribed to the (111) plane of fcc-Au, consistent with XRD analysis. Most of the particles smaller than 2 nm are Au clusters without specific crystal structure (high-angle annular dark field scanning TEM image, HAADF-STEM, Figure 1g). Au atoms were also detected, which may be stabilized at the defective sites of rGO owing to Au-O or Au-N interactions.[8a] The Au content in the composite was evaluated by thermo-gravimetric analysis, and was ~42 wt% (Figure S1, Supporting Information). According to an Au cuboctahedra model, the fraction of surface atoms on such small NPs should be close to

that of the bulk atoms, indicating that this Au catalyst may deliver a high mass activity for CO_2ER.[4a]

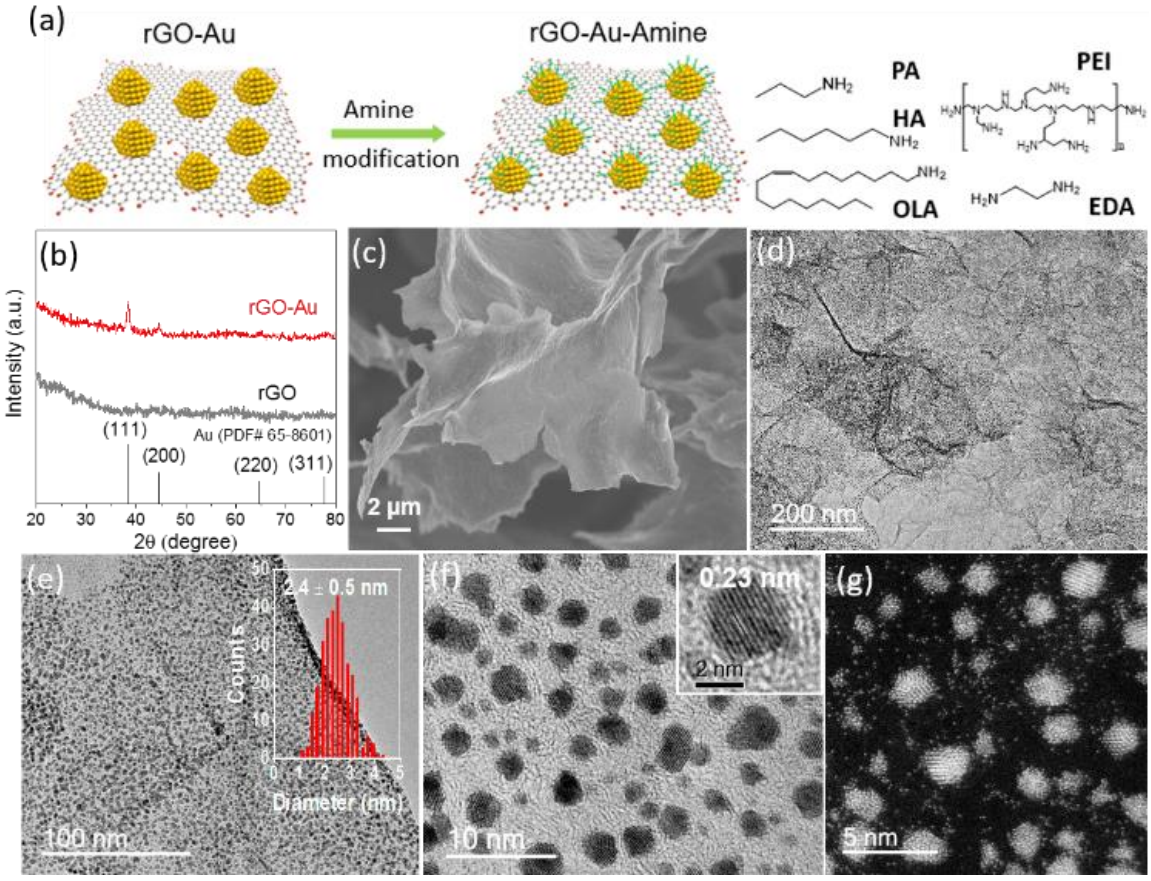

Figure 1. (a) Schematic illustration of amine modification on the rGO-Au composite; (b) XRD patterns of rGO-Au and rGO; (c) SEM and (d-e) TEM images of rGO-Au, inset of (e) histogram of Au NP sizes; (f) HRTEM and (g) HAADF-STEM images of ultrasmall Au NPs.

With the amine modification, the morphology, crystallinity and size distribution of Au NPs were nearly unchanged, yet with a moderate aggregation of the composite sheets due to the electrostatic interaction between amines and rGO sheets (Figure S2 and S3). The presence of Au clusters and single atoms were also observed (Figure S3), indicating that the interaction between Au and rGO was strong and could inhibit the detachment or severe aggregation of these Au species during amine modification. However, the structural defects on rGO were slightly reduced, as evidenced by the decreased I_D/I_G ratio in their Raman spectra in

comparison to that for rGO-Au (**Figure 2**a). This may be attributed to the decreased oxygen content on the rGO via the amine-induced ring-open reaction or nucleophilic substitution of the residual hydroxyl, epoxide and carboxyl groups.[17] Among them, OLA modified rGO-Au (simply denoted as Au-OLA) exhibited the lowest I_D/I_G ratio of 1.29, indicating its relatively low oxygen content on rGO. The attachments of amines were firstly verified by Fourier transform infrared spectroscopy (FTIR) (Figure 2b). The samples modified with bidentate EDA and polydentate PEI clearly demonstrated the characteristic bands of amines: N-H bending vibrations at 1640 - 1556 cm^{-1} and C-N stretching vibration at ~1316 cm^{-1}. The monodentate PA, HA and OLA could be discerned by the characteristic bands of C-H stretching vibration of alkane at 2840 - 2930 cm^{-1}. The surface chemical state of Au was elucidated by X-ray photoelectron spectroscopy (XPS) analysis on three representative samples, rGO-Au, Au-EDA and Au-OLA (Figure 2c). With the EDA and OLA modification, no significant binding energy shift was observed on Au^0 and Au^{3+} peaks, as that reported for N-containing ligands-functionalized Pt, Au and Ag nanostructures.[11,12a,15a] The decreased relative percentage of Au^{3+} ions might be ascribed to the strong electron donation from amine groups inducing a partial reduction.[18] The anchored amine modifiers may not be protonated in aqueous environment within the pH range of 6~8 due to the covalent-bond-like strong interaction between amine functionality and Au NPs.[18a,c,d] XPS quantification analysis demonstrated a decreased content of oxygen and an increase content of nitrogen after the EDA and OLA modification (Table S1, Supporting Information). The deconvoluted C1s spectra of Au-EDA and Au-OLA also exhibited an obvious increase in the relative percentage of C-N functionality compared with that of rGO-Au (Figure 2d). These results further evidenced the presence of amine molecules. The decreased relative content of C-OH functionality may be attributed to the reactions between amine and hydroxyl groups mentioned above.[17] This may also explain the reduced I_D/I_G ratio in the Raman analysis after amine modification.

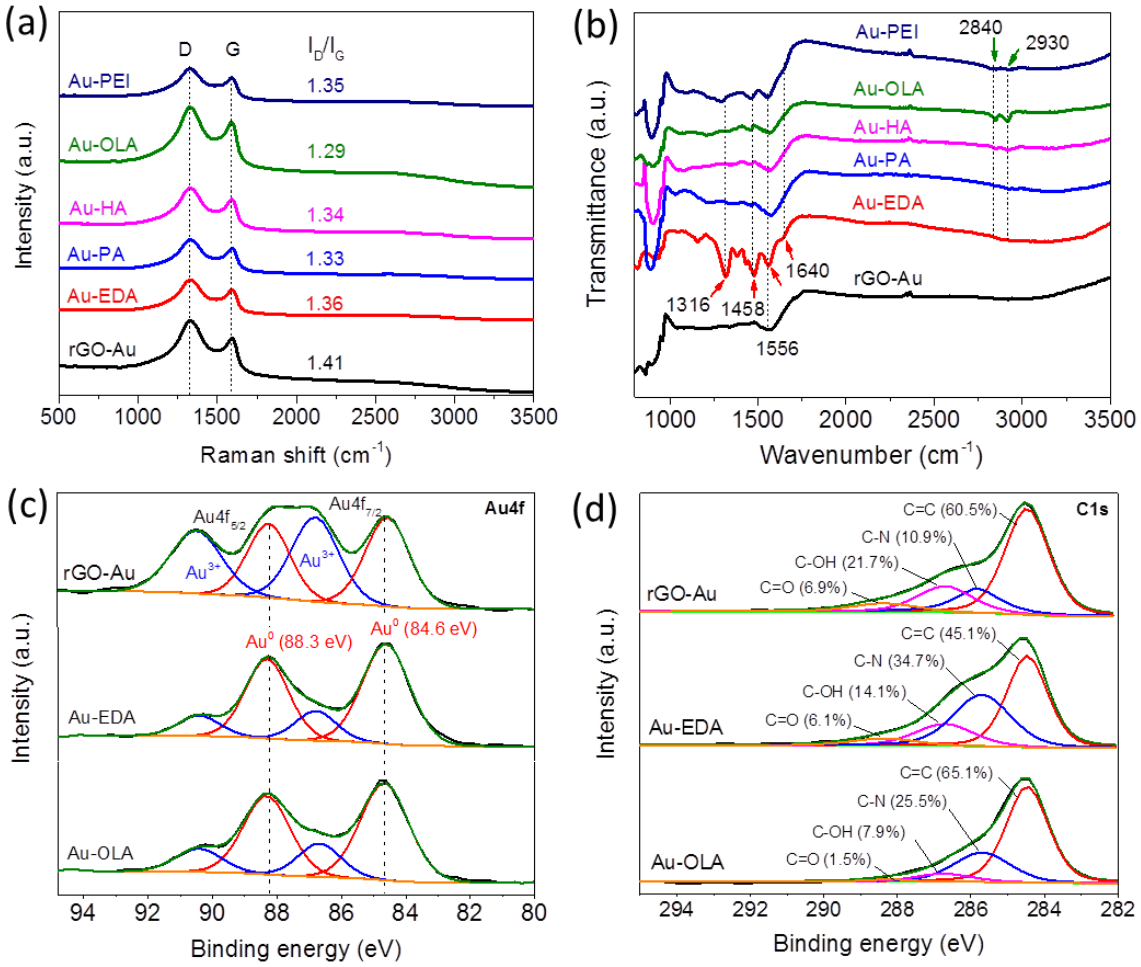

Figure 2. (a) Raman and (b) FTIR spectra of the pristine rGO-Au and five different amine modified rGO-Au; (c) Deconvoluted Au4f and (d) C1s XPS spectra of rGO-Au, Au-EDA and Au-OLA.

The CO_2ER performance of rGO-Au and the amine-modified rGO-Au catalysts were firstly evaluated by linear sweep voltammetry (LSV) studies using rGO and amine modified rGO as controls (**Figure 3**a, Figure S4a). All the catalysts containing Au exhibited much higher current densities and more positive onset potentials compared to rGO and rGO-amine samples, excluding the possibility that the superior electrocatalytic activities had arisen from rGO supports or amine modifiers. The Au-EDA and Au-PA showed similar current-voltage profiles to rGO-Au, while lower current response was observed for HA-, OLA- and PEI-modified rGO-Au (Figure 3a). The LSV trends of amine modified rGO was slightly different

from that of rGO-Au-amine (see Figure S4a and the detailed discussion in Supporting Information). To clarify the role of amine modification, controlled-potential electrolysis was performed (Figure S4b and S5). The rGO-amine samples only exhibited a current density of around 0.2 mA cm^{-2} at -0.7 V which was tens of times lower than that of Au-containing samples, further excluding the contribution of rGO-amine interactions. The iR-corrected total current densities of Au-containing samples showed similar trend to the LSV results (Figure 3b). They decreased with increasing alkyl length of amine modifiers at potentials more negative than -0.5 V (all the potentials are referenced to RHE herein) except that Au-PA exhibited the highest current densities.

The products generated were H_2 and CO. The linear amines (EDA, PA, HA and OLA) modified catalysts exhibited observably improved CO faradaic efficiencies (FE_{CO}) compared with bare rGO-Au, while the branched polyamine PEI modified catalyst (Au-PEI) remarkably hindered CO formation and improved H_2 evolution (Figure 3c, Figure S6). Among these linear amines, OLA with the longest alkyl chain exhibited the best promotion effect: FE_{CO} was improved by over 20% at the potentials more negative than -0.5 V. Specifically, at -0.6 V, the FE_{CO} of rGO-Au was only 32% and was remarkably enhanced to 59% after the OLA modification, which is even comparable to that ~60% for ultrathin Au nanowires with high density of reactive edge sites (2.1 nm width).[6] Moreover, the linear amine modification did not depress but, rather, slightly enhanced the rate of CO_2 reduction, as evidenced by the increased geometric CO partial current density (j_{CO}), in contrast to that greatly decreased j_{CO} on Au-PEI (Figure 3d). This depression effect of PEI is different from the promotion effect reported for N-doped carbon nanotubes and rGO/MoS_x,[16,13b] which may be related to the intrinsic properties of these active sites. The direct and strong interaction between PEI and ultrasmall Au NPs with abundant low-coordinated sites may induce a severe surface poisoning effect, blocking the catalytic sites for CO_2 adsorption and reduction. Figure 3e highlights the dependence of FE_{CO} and j_{CO} on the structure of amine modifiers at -0.7 V. It

clearly reveals an amine-dependent modification effect: linear amines promoted CO formation whereas the branched amine depressed it; the CO selectivity increased with the increasing alkyl chain length of linear amine modifiers. Electrochemical impedance spectroscopy was used to investigate the electron transfer and mass transportation properties of different amine modified Au catalysts, but no clear clues were observed (Figure S7).

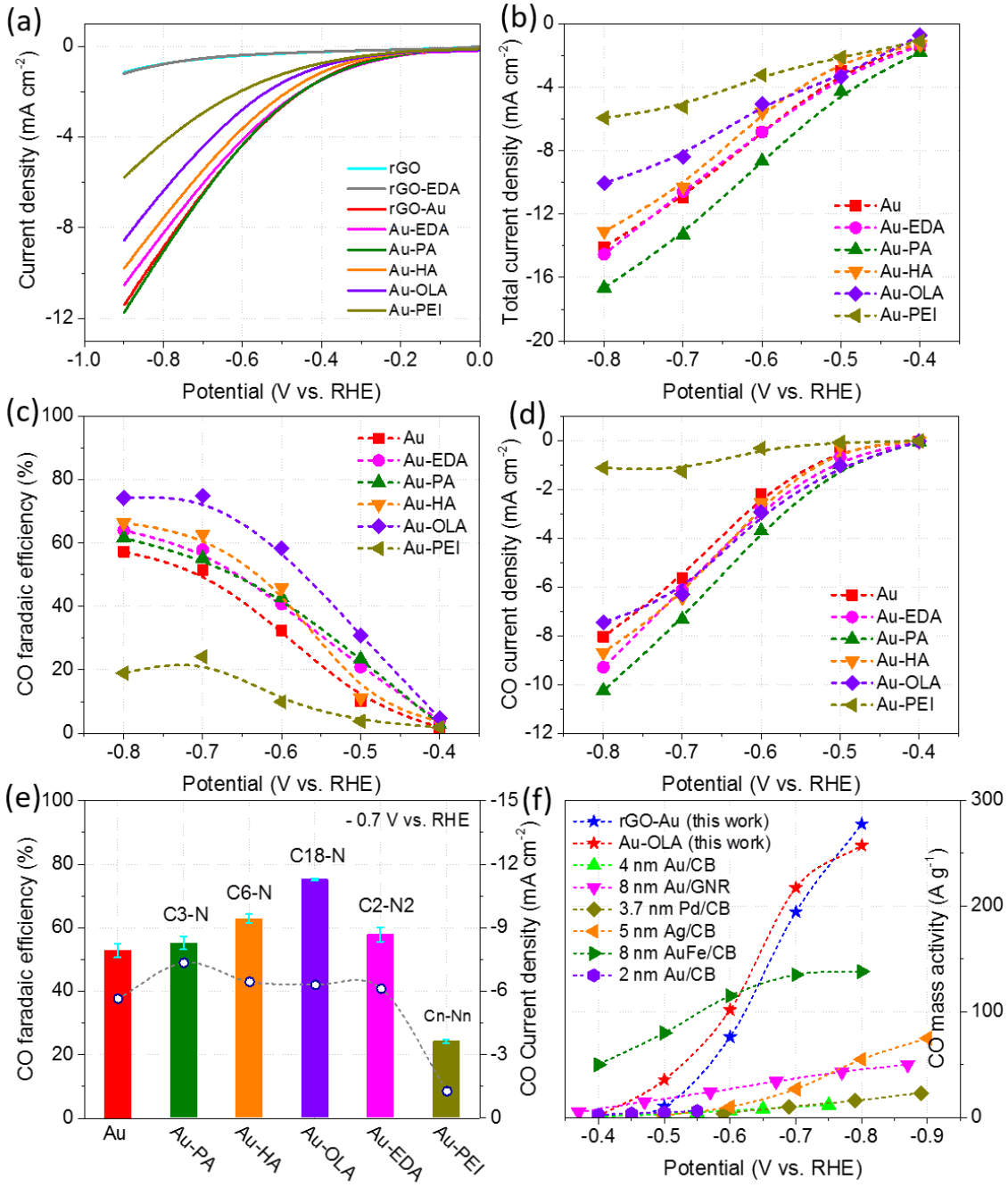

Figure 3. (a) LSV scans of rGO, rGO-EDA, rGO-Au and Au-amine in CO_2-saturated 0.1 M $KHCO_3$; (b) Geometric total current densities, (c) FE_{CO} and (d) j_{CO} at various potentials for

rGO-Au and Au-amine catalysts; (e) The FE_{CO} (column) and j_{CO} (circle) at -0.7 V; (f) Comparison of the mass activities for CO production with the reported noble metal catalysts.

The mass activity is one of the most important parameters to assess noble metallic catalysts for practical application. The OLA modified ultrasmall Au NPs delivered remarkably high mass activities for the CO_2-to-CO conversion at moderate overpotentials ranging from -0.6 to -0.8 V vs. RHE due to the intrinsic high electrocatalytic activity and high surface atom fraction (Figure 3f). A metal-specific mass activity of 102, 217 and 257 A g^{-1} was respectively obtained at -0.6, -0.7 and -0.8 V, which surpassed most of the reported noble metal catalysts such as 8 nm Au NPs on graphene nanoribbons (GNR),[19] 4 nm Au NPs on carbon black (CB),[4a] 3.7 nm Pd NPs,[20] 5 nm Ag NPs,[15a] 2 nm Au ultrathin nanowires,[6] and the benchmark catalyst 8 nm Au-Fe NPs.[21] A detailed comparison of noble metal loading and CO_2ER performance can be seen in Table S2 (Supporting Information).

Stability of the amine modification on rGO-Au for CO_2ER was investigated by comparing the Au-OLA and rGO-Au catalysts at -0.65 V, and the chronoamperometry (i-t) profiles and product selectivities were shown in **Figure 4**. Both Au-OLA and rGO-Au exhibited slightly decreasing current densities during the 10 h electrolysis with an increased FE_{CO} in the first 2 h: an increase from 64% to 68% for Au-OLA and 37% to 44% for rGO-Au. These changes may be ascribed to the slow growth of Au particle size related with aggregation.[22] The smaller change for Au-OLA indicates that OLA may stabilize the ultrasmall Au NPs. It should be pointed out that the Au-OLA catalyst did not exhibit a good stability at a more negative potential of -0.75 V, i.e., both the current density and FE_{CO} decreased gradually during the 10 h electrolysis (Figure S8). This deteriorated stability may be ascribed to the relatively severe NPs aggregation or rapid size increase at this potential. This is consistent with the reported potential-dependent growth of ligand-capped Au NPs supported on carbon

blacks, in which the growth of Au NPs in size occurred more rapidly at a more negative potential.[22a]

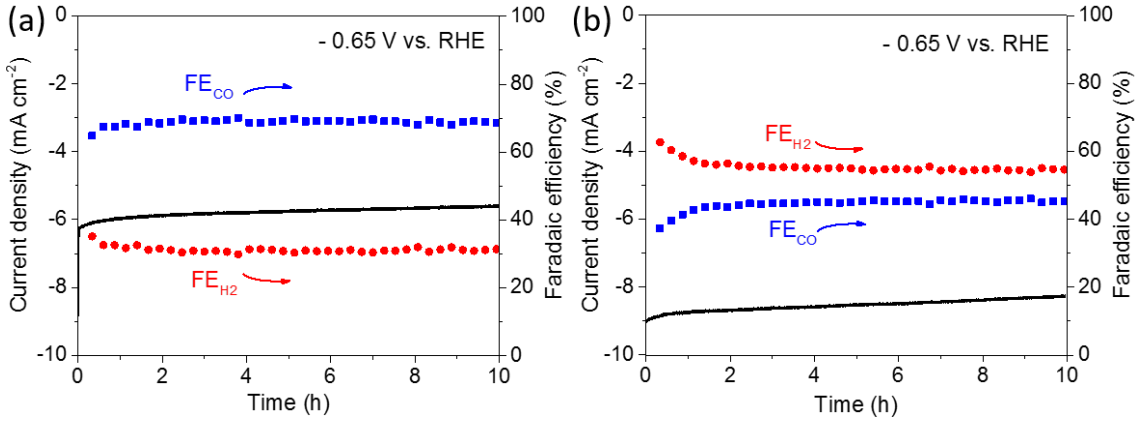

Figure 4. Stability analysis of (a) Au-OLA and (b) rGO-Au at -0.65 V for 10 h in CO_2-saturated 0.1 M $KHCO_3$.

To reveal the site-specific electrocatalytic activity, the electrochemically active surface areas (ECSAs) of Au before and after amine modification were evaluated using the Pb underpotential deposition (UPD) method (Figure S9).[12a] No obviously sharp peaks were presented on their UPD voltammograms precluding the accurate calculation of ECSAs, which is probably related to the ultrasmall size of these Au NPs. Nevertheless, Au-amine exhibited much weaker intensity compared with rGO-Au, revealing a decreased ECSA after amine modification. It can be qualitatively inferred that the ESCA-normalized j_{CO} of Au-amine is higher than that of rGO-Au, that is, the presence of amine molecules improves the site-specific catalytic activity for CO production. This is in agreement with the results for carbene-functionalized 7 nm Au NPs catalyst.[12a]

All the above results demonstrate that both the amine group and its molecular configuration greatly affect the CO_2-to-CO conversion on ultrasmall Au NPs. The promotion effect from linear amines may be explained by referencing to the reported theoretical calculation for amine-anchored Ag_{147} NPs:[15a] amine groups are more readily adsorbed on the under-coordinated corner sites of ultrasmall Au NPs, making the surrounding sites favor the

stabilization of *COOH intermediates, inhibiting the adsorption of *H and thus promoting the CO formation. To probe this further, we annealed the rGO-Au at 120 °C in air atmosphere to obtain a new composite rGO-Au120 containing large Au NPs (11.7 nm, **Figure 5**a-b) which were deficient in under-coordinated sites compared with ultrasmall Au NPs. As expected, the OLA modification on rGO-Au120 did not exhibit an obvious promotion effect, as revealed by the similar FE_{CO}, FE_{H2}, j_{H2} and j_{CO} values as the pristine samples at all the applied potentials (Figure 5c-d, Figure S10). It demonstrates the important role of Au surface structure in the amine functionalization for CO_2ER, which may be attributed to the different binding ability of amine functionality on various Au active sites such as corners, edges and facets.

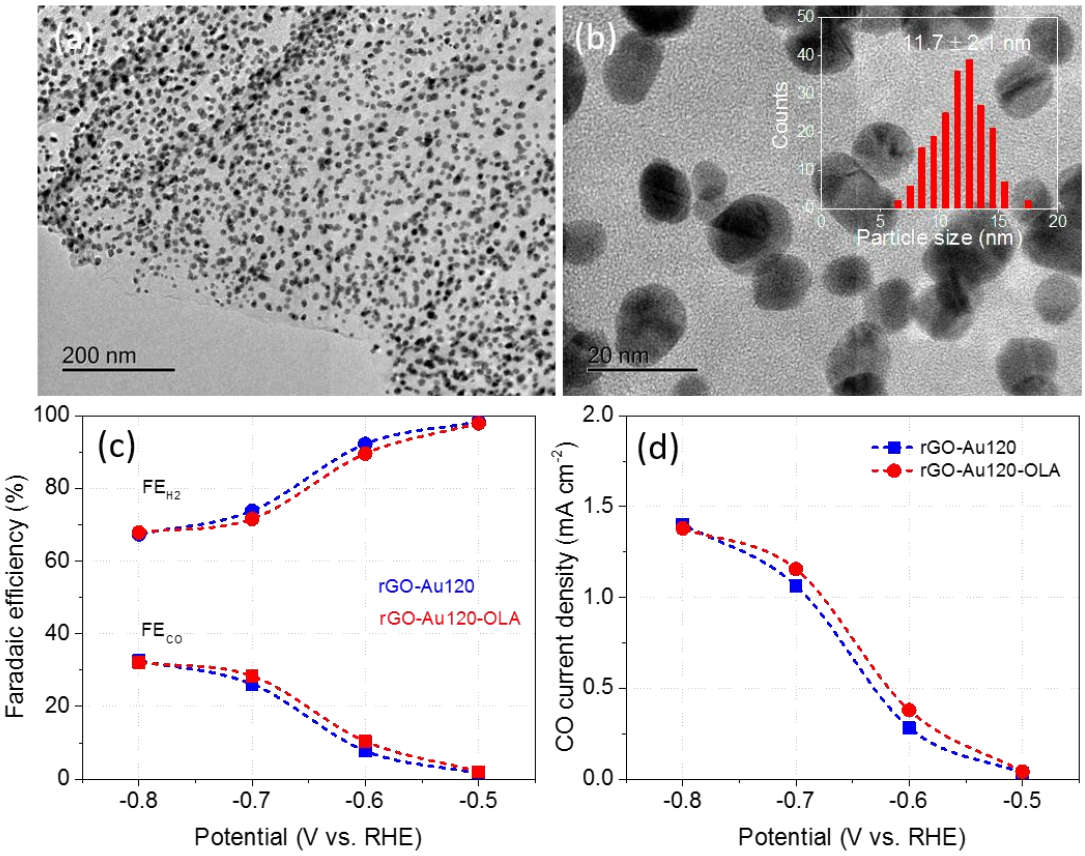

Figure 5. (a,b) TEM images of rGO-Au120 under different magnifications, inset of (b) the size distribution of Au NPs; (c) FE_{CO} and FE_{H2}, and (d) j_{CO} at various potentials for rGO-Au120 and rGO-Au120-OLA catalysts.

The influence of amine molecules on CO formation may also be related to their coverage on the ultrasmall Au NPs. As reported for CN^- and Cl^- functionalized Au electrodes, only a proper coverage of anions on Au(111) surface could benefit the CO_2ER, and higher coverages negatively affect the stabilization of *COOH and lower the activity.[12d] The amine functionality has strong electron-donating ability as well, and may induce a similar effect. However, it is challenging to quantify the amine coverage on these ultrasmall Au NPs due to the complexity of rGO-Au-amine system. Alternatively, we probed this amine-coverage effect by manipulating the purification process (i.e. removing surface modifier) of the Au-OLA catalyst. It is reasonable to infer that the Au-OLA composite via one time ethanol purification (Au-OLA-1) had a higher OLA coverage compared to that via three times (Au-OLA-3) or seven times (Au-OLA-7). Au-OLA-1 exhibited significantly depressed CO formation compared with the latter two catalysts (**Figure 6**), verifying the adverse effect of higher amine coverage for CO_2-to-CO conversion. Au-OLA-3 and Au-OLA-7 exhibited almost the same performance, indicating that a three times of ethanol washing was sufficient to remove the excessive OLA molecules on the composite. This was the condition used to prepare all the samples for CO_2ER characterizations. The PEI molecule has a branched polyamine configuration. It may induce a much higher coverage on Au sites compared with the other linear amines due to the strong Au-amine interactions and its much higher density of amine functionality, thus resulting in the greatly depressed CO formation. For the linear amines, their coverage on the Au NPs may decrease with the increasing alkyl chain length, as reported for linear thiol-ligands on Au NPs.[23] The increased CO selectivity with alkyl chain length may correlate with the decreased amine coverage on ultrasmall Au NPs.

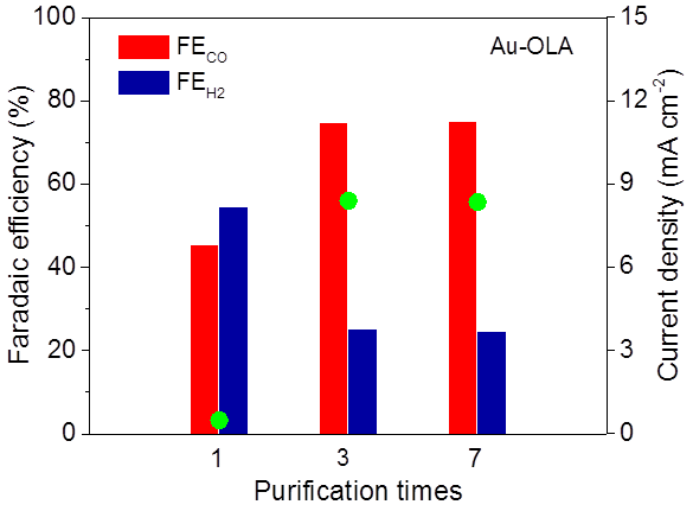

Figure 6. The CO_2ER performance of rGO-Au-OLA that was purified with ethanol for different times. Columns are the faradaic efficiencies and solid circles (green color) are the corresponding total current densities.

3. Conclusion

In summary, an ultrasmall ligand-free Au NP catalyst has been developed by a scalable rGO-assisted wet chemistry method for CO_2 electrochemical reduction with high mass activity. A simple amine modification strategy is applied to depress the severe hydrogen evolution reaction on these ultrasmall Au NPs and promote the CO_2-to-CO conversion. The amine functionality as well as the molecular configuration play important roles in tuning the electrocatalytic activity of ultrasmall Au NPs with abundant low-coordinated sites. Among all the modifiers, the linear oleylamine exhibited the most effective promotion effect on the CO selectivity probably due to its optimal coverage on the Au NPs. In addition, the surface strucuture of Au NPs such as morphology and particle size has an impact on amine functionalization due to the different binding ability of amine functionality on various Au active sites. This work may shed light on the rational design of highly efficient and selective electrocatalysts for CO_2 conversion by engineering the catalyst surface at a molecular level.

4. Experimental section

Materials. Graphite flakes (200 mesh), gold (III) chloride trihydrate (≥ 99.9%), ethylenediamine (≥ 99.5%), propylamine (≥ 99%), hexylamine (99%), oleylamine (90%), polyethylenimine (branched, average M_w ~ 800), potassium bicarbonate (≥ 99.95%), polytetrafluoroethylene dispersion (PTFE in H_2O, 60 wt%), Nafion® 117 solution (5 wt%) were purchased from Sigma-Aldrich. Carbon paper (SIGRACET® GDL 38AA, 225 ± 30 μm) was purchased from SGL Carbon GmbH. Nafion® 117 membrane was purchased from Alfa-Aesar. Ultrapure Milli-Q water (18.2 MΩ·cm) was used in this work.

Synthesis of graphene oxide (GO) and reduced graphene oxide (rGO) dispersions. The GO was prepared according to the modified Hummers method.[24] The rGO dispersions were synthesized by a simple thermal reduction method: GO (62.5 mg) was dispersed in ultrapure water (250 mL) to obtain a 0.025 wt % solution, followed by addition of ammonia solution (25 wt%, 1 mL). This mixture was heated at 95 ℃ and stirred for 3 h. After cooling to room temperature, the rGO dispersion was obtained. The mass concentration of the rGO dispersion was measured by a freeze-drying method, and it was about 0.17 mg/mL.

Synthesis of rGO-Au composite. Gold nanoparticles were synthesized on rGO sheets according to a previous report with some modifications.[8a] The $HAuCl_4$ aqueous solution (50 mM, 100 μL) was added to the freshly-prepared rGO dispersion (10 mL) under vigorous stirring at room temperature. After 15 min, the resultant products were collected by centrifugation and rinsed three times with ethanol/water (1:3 v/v) solution to remove the residual $HAuCl_4$. Sponge-like rGO-Au composite (1.67 mg) was obtained after a freeze-drying process. The content of gold in the composite was evaluated by TGA analysis, about 42 wt%. The composite of rGO-Au120 was obtained by annealing the freshly lyophilized rGO-Au composite in an oven at 120℃ for 10 h in air atmosphere. In this process, the ultrasmall Au NPs aggregated and grew into relatively large nanoparticles.

Synthesis of rGO-Au-amine composite. The obtained rGO-Au wet composite was dispersed into amine aqueous solution (0.15 M, 3 mL) and stirred for 10 min to obtain a uniform

dispersion. It was collected by centrifugation and washed with ethanol three times to remove the weakly-attached amine molecules. The rGO-Au-amine composite was obtained via lyophilisation. No obvious mass loss or gain was found after amine modification. For the modification with HA and OLA, water was replaced by an equivalent amount of ethanol to prepare the amine solution.

Synthesis of rGO-amine composites. To prepare rGO composites, the $KHCO_3$ solution (0.1 M, 2 mL) was first added into the rGO aqueous dispersion (10 mL). The flocculated rGO sheets was collected by centrifugation at 8,000 rpm for 10 min and then washed with water twice. They were modified with different amine solutions using the same procedure as above. The rGO and rGO-amine composites were obtained via lyophilisation.

Physical Characterization. XRD patterns of the catalysts were collected on a GBC MMA diffractometer with Cu Kα radiation at a scan rate of 4 degree min^{-1}. The morphology of the samples was recorded on a JEOL JSM-7500FA scanning electron microscope (SEM) and a JEOL 2010 transmission electron microscope (TEM). The dark field STEM imaging was performed on JEOL JEM-ARM200f. XPS spectra were collected on an SES2002 analyser (Scienta) with a non-monochromatic x-ray source (Omnivac) using Al Kα (1486.6 eV) radiation. Regional scans were aligned by correcting the primary C1s peak (C=C) to 284.5 eV in accordance with the literature for reduced graphite oxide.[25] Raman spectra were performed with a confocal Raman spectrometer (Jobin Yvon HR800, Horiba) using a 632.8 nm diode laser. FTIR spectra were carried out using the Shimadzu FTIR Prestige-6821 (Shimadzu Scientific Instruments, Australia). Thermal gravimetric analysis (TGA) was conducted on a Pyris Diamond thermogravimetric/differential thermal analyzer at a heating rate of 5 $^{\circ}C\ min^{-1}$ in air flow.

Fabrication of Working Electrodes. A microporous carbon black layer was painted on the surface of carbon paper (1 × 1 cm^2) by brushing an ink containing Vulcan XC72R carbon black (CB) and polytetrafluoroethylene (PTFE). The CB loading was ~0.9 mg cm^{-2}, and the

PTFE content was ~15 wt%. The catalyst ink was prepared by mixing 1.67 mg of rGO, rGO-amine, rGO-Au or rGO-Au-amine composite, 1.8 mL of ethanol/water (2:3 v/v) solution and 0.1 mL Nafion solution (5 wt%) with ultrasonication for 15 min. An aliquot of the catalyst ink (70 μL) was dropped evenly on the CB layer (1cm^2) and kept at room temperature overnight to evaporate most of the solvents. Working electrodes were obtained by annealing them at 70 °C for 3 h. The loading mass of composite catalyst was about 71 μg cm^{-2}, and the Au loading in Au-containing electrodes was then calculated to be about 30 μg cm^{-2}. For the rGO-Au120 and rGO-Au120-OLA electrodes, the loading mass of composites was increased to 112 μg cm^{-2} to improve the response current due to the poor electrocatalytic activity of large Au NPs.

Electrochemical measurements. All the experiments were carried out on a potentiostat (CHI 650D) in a two-compartment gastight glass H-cell. The cathodic and anodic compartments were separated by a piece of Nafion membrane. Each compartment holds 30 mL of electrolyte and leaves a headspace of about 20 mL. A piece of platinum gauze (2 cm × 2 cm) and an Ag/AgCl electrode served as counter electrode and reference electrode respectively. The 0.1 M $KHCO_3$ aqueous solution was used as electrolyte directly without any purification. All the potentials were corrected using automatic iR compensation function on the potentiostat. The potentials were measured against reference electrode and converted to reversible hydrogen electrode (RHE) reference scale by the following equation, $E_{RHE} = E_{Ag/AgCl} + 0.21 + 0.0591 \times pH$. The pH value of CO_2-saturated 0.1 M $KHCO_3$ aqueous solution is 6.78. The current density reported in this work was normalized to the geometric surface area.

Prior to the CO_2 reduction, the cathodic electrolyte was saturated with CO_2 (99.99%, BOC Australia) at a flow-rate of 20.0 mL min^{-1} controlled by a mass flow controller (GFC17, Aalborg®) for at least 20 min under a stirring rate of 500 rpm. Linear sweep voltammetry was conducted initially at a scan rate of 20 mV s^{-1}. During the chronoamperometry electrolysis,

CO_2 was continuously bubbled into the cathodic compartment and vented directly into the gas-sampling loop (1 mL) of a gas chromatograph (8610C, SRI). The gas chromatograph was equipped with a packed MolSieve 5A column (1/8" × 6') and a packed Haysep D column (1/8" × 6') with argon flowing as carrier gas. The separated gases were analyzed by a thermal conductivity detector (for H_2) and a flame ionization detector with methanizer (for CO). Quantification of the products was performed by an external standard method.[26,1b] A standard gas mixture composed of H_2, CO, CH_4, C_2H_4 and CO_2 (BOC Australia) was used to obtain the calibration curve for H_2 and CO. The first GC run was initiated at the 10th min, and thereafter re-initiated every 16 min twice more. The average of the results from three measurements was used for the data analysis. Liquid products were analysed afterwards on a 400 MHz NMR spectrometer (Bruker Avance) and quantified according to our previous report.[26,1b] The faradaic efficiencies (FEs) were calculated from the amount of charge passed to produce each product divided by the total charge passed at a specific time. The FEs were finally normalized to the reported values based on a total FEs of 100% at each potential.

Supporting Information

Supporting Information is available from the Wiley Online Library or from the author.

Acknowledgements

Funding from the Australian Research Council Centre of Excellence Scheme (CE 140100012) is acknowledged. The authors thank Australian National Fabrication Facility-Materials Node (ANFF) and UOW Electron Microscopy Centre for equipment use.

Received: ((will be filled in by the editorial staff))
Revised: ((will be filled in by the editorial staff))
Published online: ((will be filled in by the editorial staff))

References

[1] a) J. Qiao, Y. Liu, F. Hong, J. Zhang, *Chem. Soc. Rev.* **2014**, *43*, 631-675; b) Y. Zhao, C. Wang, G. G. Wallace, *J. Mater. Chem. A* **2016**, *4*, 10710-10718.

[2] E. E. Benson, C. P. Kubiak, A. J. Sathrum, J. M. Smieja, *Chem. Soc. Rev.* **2009**, *38*, 89-99.

[3] Y. Hori, In *Modern aspects of electrochemistry*; Springer: **2008**, pp. 89-189.

[4] a) W. Zhu, R. Michalsky, O. N. Metin, H. Lv, S. Guo, C. J. Wright, X. Sun, A. A. Peterson, S. Sun, *J. Am. Chem. Soc.* **2013**, *135*, 16833-16836; b) Y. Chen, C. W. Li, M. W. Kanan, *J. Am. Chem. Soc.* **2012**, *134*, 19969-19972; c) X. Feng, K. Jiang, S. Fan, M. W. Kanan, *J. Am. Chem. Soc.* **2015**, *137*, 4606-4609; d) D. Kim, J. Resasco, Y. Yu, A. M. Asiri, P. Yang, *Nat. Comm.* **2014**, *5*, 4948.

[5] A. S. Hall, Y. Yoon, A. Wuttig, Y. Surendranath, *J. Am. Chem. Soc.* **2015**, *137*, 14834-14837.

[6] W. Zhu, Y.J. Zhang, H. Zhang, H. Lv, Q. Li, R. Michalsky, A. A. Peterson, S. Sun, *J. Am. Chem. Soc.* **2014**, *136*, 16132-16135.

[7] M. Liu, Y. Pang, B. Zhang, P. De Luna, O. Voznyy, J. Xu, X. Zheng, C. T. Dinh, F. Fan, C. Cao, *Nature* **2016**, *537*, 382-386.

[8] a) H. Yin, H. Tang, D. Wang, Y. Gao, Z. Tang, *ACS Nano* **2012**, *6*, 8288-8297; b) X.F. Yang, A. Wang, B. Qiao, J. Li, J. Liu, T. Zhang, *Acc. Chem. Res.* **2013**, *46*, 1740-1748; c) Y. J. Wang, D. P. Wilkinson, J. Zhang, *Chem. Rev.* **2011**, *111*, 7625-7651.

[9] a) Z. Wu, D.E. Jiang, A. K. Mann, D. R. Mullins, Z.A. Qiao, L. F. Allard, C. Zeng, R. Jin, S. H. Overbury, *J. Am. Chem. Soc.* **2014**, *136*, 6111-6122; b) D. Li, C. Wang, D. Tripkovic, S. Sun, N. M. Markovic, V. R. Stamenkovic, *ACS Catal.* **2012**, *2*, 1358-1362.

[10] H. Mistry, R. Reske, Z. Zeng, Z.J. Zhao, J. Greeley, P. Strasser, B. R. Cuenya, *J. Am. Chem. Soc.* **2014**, *136*, 16473-16476.

[11] G. Chen, C. Xu, X. Huang, J. Ye, L. Gu, G. Li, Z. Tang, B. Wu, H. Yang, Z. Zhao, *Nat. Mat.* **2016**, *15*, 564-569.

[12] a) Z. Cao, D. Kim, D. Hong, Y. Yu, J. Xu, S. Lin, X. Wen, E. M. Nichols, K. Jeong, J. A. Reimer, P. Yang, C. J. Chang, *J. Am. Chem. Soc.* **2016**, *138*, 8120-8125; b) Y. Fang, J. C. Flake, *J. Am. Chem. Soc.* **2017**, *139*, 3399-3405; c) D. R. Kauffman, D. Alfonso, C. Matranga, H. Qian, R. Jin, *J. Am. Chem. Soc.* **2012**, *134*, 10237-10243; d) M. Cho, J. T. Song, S. Back, Y. Jung, J. Oh, *ACS Catal.* **2018**, *8*, 1178-1185.

[13] a) C. Kim, H. S. Cho, S. Chang, S. J. Cho, M. Choi, *Energy Environ. Sci.* **2016**, *9*, 1803-1811; b) F. Li, S.F. Zhao, L. Chen, A. Khan, D. R. MacFarlane, J. Zhang, *Energy Environ. Sci.* **2016**, *9*, 216-223; c) B. Rezaei, S. Mallakpour, M. Taki, *J. Power Sources* **2009**,*187*, 605-612; d) B. A. Rosen, W. Zhu, G. Kaul, A. Salehi-Khojin, R. I. Masel, *J. Electrochem. Soc.* **2012**, *160*, H138-H141.

[14] a) M. S. Xie, B. Y. Xia, Y. Li, Y. Yan, Y. Yang, Q. Sun, S. H. Chan, A. Fisher, X. Wang, *Energy Environ. Sci.* **2016**, *9*, 1687-1695; b) A. S. Varela, W. Ju, T. Reier, P. Strasser, *ACS Catal.* **2016**, *6*, 2136-2144.

[15] a) C. Kim, T. Eom, M. S. Jee, H. Jung, H. Kim, B. K. Min, Y. J. Hwang, *ACS Catal.* **2016**, *7*, 779-785; b) Y.C. Hsieh, S. D. Senanayake, Y. Zhang, W. Xu, D. E. Polyansky, *ACS Catal.* **2015**, *5*, 5349-5356; c) C.Y. Lee, Y. Zhao, C. Wang, D. R. G. Mitchell, G. G. Wallace, *Sustainable Energy Fuels* **2017**,*1*, 1023-1027.

[16] S. Zhang, P. Kang, S. Ubnoske, M. K. Brennaman, N. Song, R. L. House, J. T. Glass, T. J. Meyer, *J. Am. Chem. Soc.* **2014**, *136*, 7845-7848.

[17] L. Lai, L. Chen, D. Zhan, L. Sun, J. Liu, S. H. Lim, C. K. Poh, Z. Shen, J. Lin, *Carbon* **2011**, *49*, 3250.

[18] a) A. Kumar, S. Mandal, P. R. Selvakannan, R. Pasricha, A. B. Mandale, M. Sastry, *Langmuir* **2003**, *19*, 6277-6282; b) T. Bligaard, J.K. Nørskov, *Electrochimica Acta* **2007**, *52*, 5512-5516; c) M. Aslam, L. Fu, M. Su, K. Vijayamohananb, V. P. Dravid,

J. Mater. Chem. **2004**,*14*, 1795-1797; d) D. V. Leff, L. Brandt, J. R. Heath, *Langmuir* **1996**, *12*, 4723-4730.

[19] C. Rogers, W. S. Perkins, G. Veber, T. E. Williams, R. R. Cloke, F. R. Fischer, *J. Am. Chem. Soc* **2017**, *139*, 4052-4061.

[20] D. Gao, H. Zhou, J. Wang, S. Miao, F. Yang, G. Wang, J. Wang, X. Bao, *J. Am. Chem. Soc.* **2015**, *137*, 4288-4291.

[21] K. Sun, T. Cheng, L. Wu, Y. Hu, J. Zhou, A. MacLennan, Z. Jiang, Y. Gao, W. A. Goddard, Z. Wang, *J. Am. Chem. Soc.* **2017,** *139*, 15608-15611.

[22] a) J. A. Trindell, J, Clausmeyer, R. M. Crooks, *J. Am. Chem. Soc.* **2017**, *139*, 16161-16167; b) P. J. Ferreira, G. J. la O, Y. Shao-Horn, D. Morganb, R. Makharia, S. Kocha, H. A. Gasteiger, *J. Electrochem. Soc.* **2005**, 152, A2256-A2271.

[23] H. Hinterwirth, S. Kappel, T. Waitz, T. Prohaska, W. Lindner, M. Lämmerhofer, *ACS Nano* **2013**, *7*, 1129-1136.

[24] Y. Liu, B. Weng, J. M. Razal, Q. Xu, C. Zhao, Y. Hou, S. Seyedin, R. Jalili, G. G. Wallace, J. Chen, *Sci. Rep.* **2015**, *5*, 17045.

[25] C. Teng, C. M. Ma, C. Hua Lu, S. Yang, S. Lee, M Hsiao, M. Yen, K. Chiou, T. Lee *Carbon* **2011**, *49*, 5107.

[26] Y. Zhao, J. Liang, C. Wang, J. Ma, G. G. Wallace, *Adv. Energy Mater.* **2018**, 1702524.